In-situ Synthesis of KO_2 Nanocrystals on Porous Fiberglass Matrix as an Air Regenerative Product

Chegeni, Asma; Babaeipour, Valiollah*[+]; Fathollahi, Manoochehr; Hosseini, Seyed Ghorban

Faculty of Chemistry and Chemical Engineering, Malek-Ashtar University of Technology, Tehran, I.R. IRAN

ABSTRACT: *The in-situ synthesis of KO_2 nanocrystals on a porous fiberglass matrix is a promising route for the development of air regenerative products such as chemical lungs. The preparation process was studied experimentally with Taguchi experimental design L_{18} orthogonal array (3^5) to examine the effect of five physicochemical variables at three levels. Maximum active oxygen content (O_{act} wt.%) as the objective of optimization was determined by hot air at a temperature of 120 °C, flow rate 325 L/min, time of 10 min with 10 cm distance from the matrix, and alkaline solution 1.5%. The analysis of variance (ANOVA) with Fisher's test revealed that the hot air temperature has the most significant effect on the response. The XRD pattern and TGA decomposition curves of the optimal sample confirmed the form of KO_2 nanocrystals as a major phase on the matrix. The morphology and elemental analysis of the product determined by FESEM and EDX analysis have been evenly distributed both in pores and on the surface of the matrix in the form of spherical or quasispherical grains (10-40 nm in diameter). The BET-specific surface area of KO_2 nanocomposite was measured about at 1.252 m^2/g and they have a mesoporous solid structure. The best CO_2 adsorption kinetic model was the Elovich model which fits the experimental kinetic data. The thermodynamic parameters represent the spontaneous and exothermic processes.*

KEYWORDS: *Air revitalization system; KO_2 nanocomposite; In-situ synthesis; Taguchi statistical design; Kinetics; Thermodynamic; Modeling.*

INTRODUCTION

Potassium and sodium superoxide are the main constituents of air regenerative products in life support systems. These materials can protect humans against undesirable atmospheric conditions and can be used as a chemical lung [1, 2]. These chemicals have excellent potential to chemisorb the moist CO_2 and simultaneously generate oxygen required for breathing. The KO_2 can provide System Respiratory Quotients (SRQ) of up to 0.82, adequate for Man Respiratory Quotients (MRQ) [3-6].

The KO_2 can be produced by different synthesis procedures. The oxidation of potassium in an oxygen medium is a commonly applied technique in Russia and China. The disadvantages of this method are the high cost, handling, and storage of the product. On the other hand in France, the reactants were mixed in halogenated hydrocarbons as reaction buffers and cooling accelerators. The mixture is subsequently pyrolyzed under atmospheric pressure. However, the purity of the products with this

*** To whom correspondence should be addressed.*

+ E-mail: vbabaeipour@mut.ac.ir

1021-9986/2022/11/3521-3541 21/$/7.01

route is not competitive with the previous method. The third method is based on a wet process in which potassium hydroxide reacts with hydrogen peroxide followed by dehydration of potassium peroxide per oxo hydrates using hot dry airflow. This latter method is commonly applied in Germany and the USA, which has been subject to various modifications such as solution preparation under vacuum and desiccation over concentrated sulfuric acid [7-9].

To reduce production losses and improve the performance of air regenerative products, environmentally friendly technology for manufacturing air regenerative products has been developed by randomly cross-linking KO_2 nanocrystals on a high porosity fiberglass matrix [10, 11].

The produced material has a large surface area. This property facilitates the effective access of water vapor and CO_2 to every crystal of KO_2. It can be easily produced within plates of any thickness. This method can significantly reduce metal consumption (50–90%), rubber materials (15–25%), and consequently the load of the ultimate products about ~1.5–2 times [12, 13]. The material is prepared in two steps of impregnation a fiberglass matrix with a solution of potassium peroxide peroxo hydrate, $K_2O_2{\cdot}2H_2O_2$, (Reaction 1) and dehydration of this high moisture material in a vacuum under heating (Reaction (2)) [14].

$$2KOH + 3H_2O_2 \rightarrow K_2O_2.2H_2O_2 + 2H_2O \quad (1)$$

$$K_2O_2.2H_2O_2 \rightarrow 2KO_2 + 2H_2O \quad (2)$$

The KO_2 production from the intermediate solution may be the complicated stage of this technique because the highly exothermic reaction of H_2O_2 with KOH causes a considerable loss of oxygen [15]. The influence of water on hyper oxide makes it necessary to conduct the disproportionate reaction in an apparatus permitting the separation of KO_2 from the reaction water as rapidly as possible. The third difficulty is the side reaction of CO_2 with KO_2 and consequent consumption of the potassium peroxide during the manufacturing process, which makes it necessary to perform all the stages in an atmosphere free from CO_2. The general equation of this probable process is as follows [16]:

$$mK_2O_2.2H_2O_2 \rightarrow nKO_2 + (m-n)KOH + H_2O + O_2 \quad (3)$$

Using the appropriate drying method and also changing the drying process parameters, the ratio of KO_2 and KOH in the final product can be controlled on the porous matrix. Therefore, during the synthesis of the KO_2 powder at medium and high temperatures, any adverse reactions may occur that are unavoidable. So far, the selection of appropriate processing techniques for KO_2 powder is a researchers' challenge [17]. Today, various methods for drying KO_2 powder on polymer matrix have been proposed to produce high-quality air regenerative products. These methods include drying with IR waves under vacuum, drying with hot air under atmospheric pressure, drying with the use of heat resistance, and drying in the microwave [14, 18].

The present work aimed to optimize influential factors employing a design of experiment (DOE) methodology the process of in-situ synthesis of pure KO_2 nanocrystals by drying at atmospheric pressure with heated air. To investigate this opinion, optimizing the five influential factors on the in-situ synthesis of nanocomposites through a Design of Experiment (DOE) methodology has been opted as the objective of this research. DOE methodology by Taguchi Orthogonal Array (OA) can efficiently determine optimum experimental parameters by analyzing response and quality. Analysis of the experimental data using ANOVA (analysis of variance) provides information about statistically significant factors and their optimum levels for the planning of experimental parameters[19, 20].

The KO_2 nanocomposites can be considered as adsorbent substrates that can chemically adsorb carbon dioxide to create the desired atmosphere in closed atmospheres [21]. Therefore, it is necessary to study the adsorption kinetics to determine the adsorbent efficiency and also to predict the adsorption rate as one of the most important factors required to design an optimal air revitalization system [22, 23]. Another important criterion in describing the adsorption process is to determine the thermodynamic parameters of adsorption, which reflects the spontaneity of the processes, the endothermic or exothermic reaction, and the entropy changes during the adsorption process [24]. In this study, for the first time, the CO_2 adsorption kinetics and thermodynamic models on optimal KO_2 nanocomposites which were synthesized by an effective approach have been investigated.

EXPERIMENTAL SECTION

Materials

The KOH 90% (W/W), H_2O_2 50% (V/V), $MgSO_4$, and Co $(NO_3)_2$ were bought from Merck (Darmstadt, Germany) in analytical reagent grades. The flake potash

containing up to 10 ppm of Fe^{2+} and/or Fe^{3+} cations was used in a commercial grade and preferably dry form. The de-ionized water was used throughout the experiments. Commercial fiberglass was purchased from Qinhuangdao Dinuo technology Development Co. and was used as high-porosity polymeric support.

Drying equipment

A German-made heat gun was applied for all the drying and aeration processes of the impregnated bed under air pressure. This heat gun Metabo, HE 23-650, provides hot air within the temperature range of 50 to 650 °C and hot air blowing speed of 150 to 500 L/min, with the power of 2300 W.

The in-situ synthesis

This reaction is strongly exothermic under normal conditions, and which makes decomposition of the products and evolution of atomic oxygen. Hence, it's essential either to chill the reaction area, which needs power consumption or to feature a stabilizer. The acceptable stabilizer, which is kept available oxygen in alkaline solution for an extended time, should complete individual commitments concerning their toxicity, thermal stability, chemical resistance to atomic oxygen, etc.

If even a couple of impurities are present within the solution, hydrogen peroxide quickly loses the oxygen of the solvent, therefore the selection of the matrix for the in situ synthesis of regenerative products is extremely important. Therefore, the matrix has the subsequent properties: porous, hydrophilic and, versatile, having an oxygen index of about 100%, thermal stability, non-combustible in touch with active oxygen-containing materials, permeable, inert, and immune to alkaline and oxidizing agents. In this way, the kinds of glass structures, including the mat, needle mat, and wool, were compared during a series of separate experiments. Finally, glass wool with the highest porosity, hydrophilicity, maximum heat resistance, and terminal flexibility was selected because of the base matrix and used in all operations. This white matrix with unidirectional weave patterns has aerial weight around 200-880 g/m^2, density 2.55 gr/cm^3, and fabric thickness around 0.16-0.34 mm. The glass wool was first washed with an alkaline solution (5% W/V, NaOH) to get rid of oil within the structure, then neutralized with an acidic solution (2% V/V, HNO_3), then the cleaned polymer was calcined at 300 °C for 12 h and eventually washed with distilled water. The sample was dried at high temperature and prepared in proper dimensions (5×5 mm) [14].

The potassium hydroxide and hydrogen peroxide were mixed and reacted in a vessel submerged in an ice bath, under a temperature below a critical temperature and highly reduced pressure. This low temperature decreases the chances of explosion by partly slowing down the extreme reaction between the H_2O_2 and KOH, without noticeably lengthening the operation time. Upon adding the last addition of the H_2O_2, the reaction mixture is stirred until the end of the reaction. To be sure of the purity of the raw materials, every component was monitored weekly consistent with the standard laboratory procedures (H_2O_2 and KOH were respectively titrated with standard permanganate solution and sulfuric acid) before each test.

To impregnate the porous fiberglass matrix with KO_2 nanocrystals, the intermediate $K_2O_2.2H_2O_2$ solution (Reaction 1) was sprayed on the glass wool and then dehydrated by heating in a vacuum. To increase the porosity of the final nanocomposites, the heating was done by the heat gun with an aeration pattern perpendicular to the bed surface[25]. Fig. 1 shows the schematic of the synthesis procedure developed for the production of the KO_2 nanocrystals.

The ratio of KO_2 and KOH in the final porous KO_2 nanocomposite can be controlled by changing the process parameters including the drying procedure and combination of the intermediate solution. The weight of the final product was determined by measuring before and after impregnation and after the synthesis of KO_2 nanocrystals.

Determination of the active oxygen

Respiration in the human lung occurs through the exchange of fresh oxygen to the red blood cells of the arteries and the uptake of carbon dioxide produced by the cells. However, in the chemical lung, this process takes place through the use of air-reducing compounds. Nanocrystals of potassium superoxide is a strong candidate for use in Air Revitalization Systems (ARS) because it efficiently not only captures CO_2 present in air but also generates O_2. The process of respiration in porous KO_2 nanocomposite as a chemical lung follows the following reaction:

$$2KO_2 + H_2O \rightarrow 2KOH + 3/2O_2 \quad (4)$$

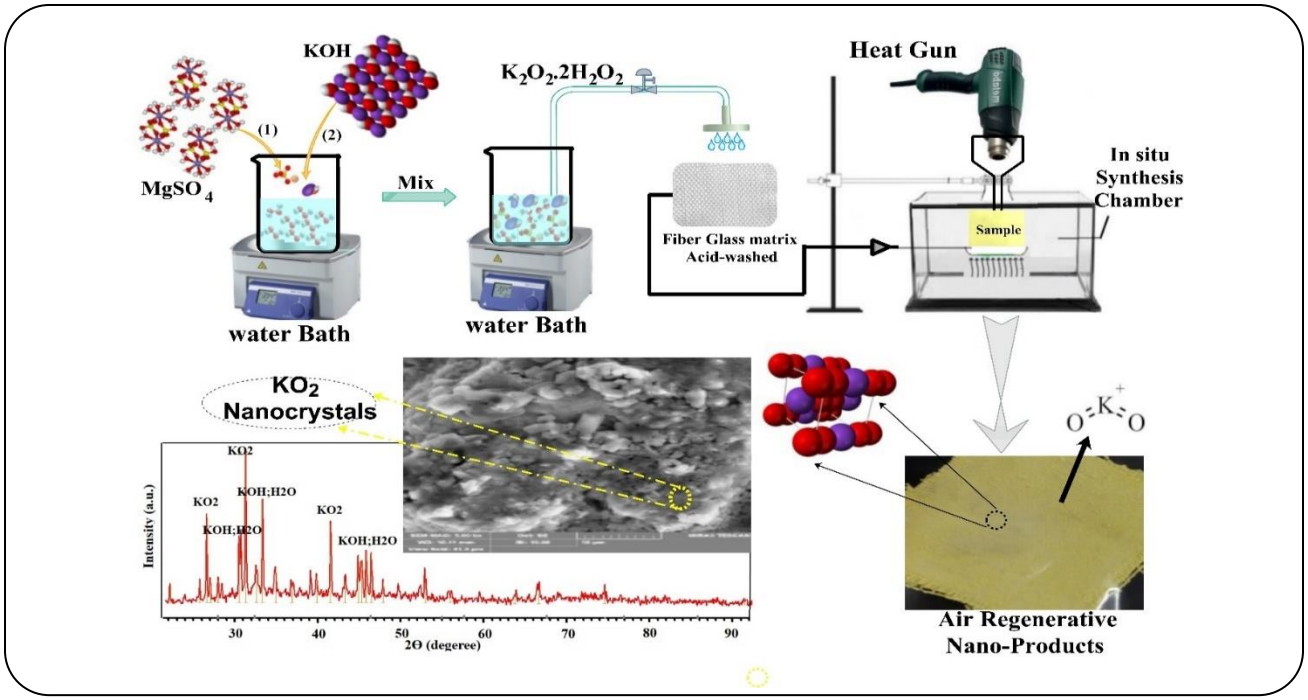

Fig. 1: Schematic of the in-situ synthesis procedure of potassium superoxide nanocrystals.

$$2KOH + CO_2 \rightarrow K_2CO_3 + H_2O \quad (5)$$

$$2KO_2 + CO_2 \rightarrow K_2CO_3 + 3/2O_2 \quad (6)$$

As depicted in Fig. 2, CO_2 by absorbing water vapor is converted into O_2 in the presence of KO_2 nanocomposite in the chemical lung. The active oxygen was determined based on the reaction between KO_2 and an aqueous solution of cobalt nitrate. The outcome of this reaction ends up with the release of gaseous oxygen [1]. Thus, a sample with a mass of 0.2 to 0.4 g KO_2 nanocrystals was placed in 10 mL of 5 vol% $Co(NO_3)_2$. The quantity of reactive oxygen was then calculated by determining the weight lost as follows [26]:

$$Q_{act}\,(wt\%) = \frac{W_i - W_f}{W_i} \times 100 \quad (7)$$

Where, O_{act} (*wt. %*) is the active oxygen in air revitalization KO_2 nanocomposite W_i and W_f are the weight of the air revitalization products and the one after placing in the aqueous solution of cobalt nitrate, respectively [27].

Experimental design for in-situ synthesis

The effects of five physicochemical variables on the synthesis process were investigated at three levels by the Taguchi method [28]. These factors are the molar ratio of hydrogen peroxide to potassium hydroxide (1.5,1.75,2%) as a chemical factor and four physical parameters including temperature (120,130,140°C), time (10,15,20 min), the hot air flow rate (220,325,430 L/min), and the aeration distance from the surface of the matrix (5,10,15 cm). The experimental design was planned by MINITAB software (version 19.2, Minitab Inc., State College, PA, USA). The L_{18} (3^5) orthogonal array experiments were designed to achieve a consistent distribution under experimental control factors (Table 1). Orthogonal arrays exhibit self-balancing properties and make up only a fraction of full factorial experiments. A p-value of less than 0.05 was considered a statistically significant difference. The experiments were carried out based on the designed L_{18} (3^5) orthogonal array at least twice.

The Signal-to-Noise Ratio (SNR) is of crucial significance in adjusting the standard of output. This ratio was considered an optimization objective in the Taguchi method and estimated by calculating the adjusted mean square deviation of the average quality loss function. By comparing the plots of the SNRs for each factor, the optimum value can be determined [29]. The noise in this study was designated as the amount of white by-product (KOH) obtained by the side reaction. For this plan,

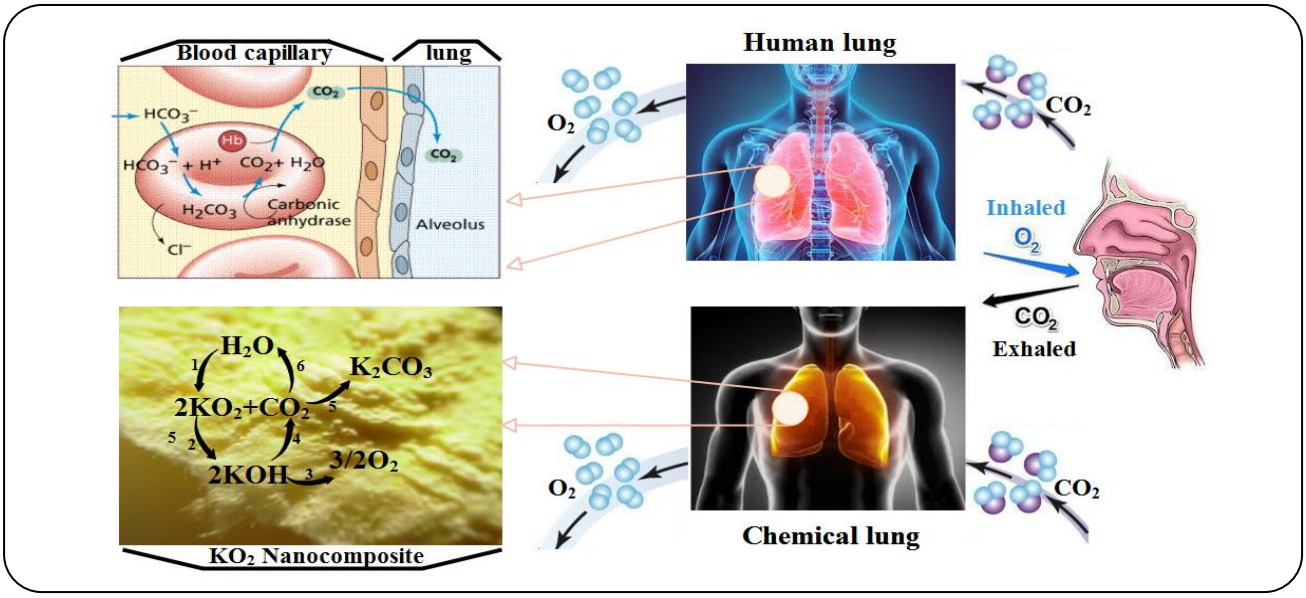

Fig. 2: Compare the process of converting CO_2 into O_2 in human and lung chemicals.

the amount of yellow product (KO_2) composed on the matrix from the reaction (Reaction 3) was considered as the response (signal). The SNR was calculated as follows [30, 31]:

$$\frac{S}{N} = -10\log\left[\frac{1}{n}\sum_{i=1}^{n}\left(\frac{1}{Y_i^2}\right)\right] \quad (8)$$

Where the S/N ratio is calculated from observed values of Q_{act} (%). Y_i represents the experimentally observed value of the i^{th} experiment, and n is the repeated number of every trial. Notably, each experiment in the L_{18} array is conducted three times.

Characterization

The optimum sample of porous KO_2 nanocomposite was characterized by different analytical techniques of X-Ray Diffraction (XRD), Field Emission Scanning Electron Microscopy (FESEM), Energy-Dispersive X-ray (EDX), Brauer–Emmett–Teller (BET) surface area, and ThermogGravimetry/Differential Thermal Analysis (TG/DTA). The XRD analysis on a D2 phase diffractometer (Netherlands, Philips, Cu radiation, 1.54056 Å) was determined to understand the qualitative phase composition of crystals and crystalline phases. Intensity data were collected in the angular range (2θ) 5° to 100° at a scan step of 0.02°. The FESEM analysis was done by MIRA III (TE-SCAN, Czech Republic) to examine surface morphology and the pore structure of the nanocrystals. Also, a SAMX Detector (TESCAN, Czech Republic) was used to figure out the surface composition of the synthesized nanocrystals by EDX-Dot mapping analysis. To examine the texture properties, the BET Specific Surface area (SBET) and the pore volume (V pore) for the chemical lung were measured step by step through BELSORP MINI II (Crea Laboratory Technologies, Japan). The thermal stability of the optimum sample was examined by a Q600 TGA instrument (TA, USA) in the temperature range of 40–550°C at a continuous heating rate of 10 °C/min. The test was done under nitrogen airflow for all samples.

Kinetic behavior and thermodynamic studies of CO_2 adsorption

Absorption kinetics describes the reaction path and the equilibrium time. The study of adsorption kinetics indicates the adsorption efficiency, and the adsorption of the adsorbent on the adsorbent may involve one or more stages, including film diffusion, intraparticle diffusion, surface diffusion, and adsorption at the pore surface, or a combination of several steps. Adsorption kinetics depends on the physical and chemical properties of the adsorbent that affect the adsorption mechanism[32, 33]. Kinetic models are used to investigate the adsorption mechanism and calculate the adsorption rate. They are also used to study potential rate-controlling steps[34, 35].

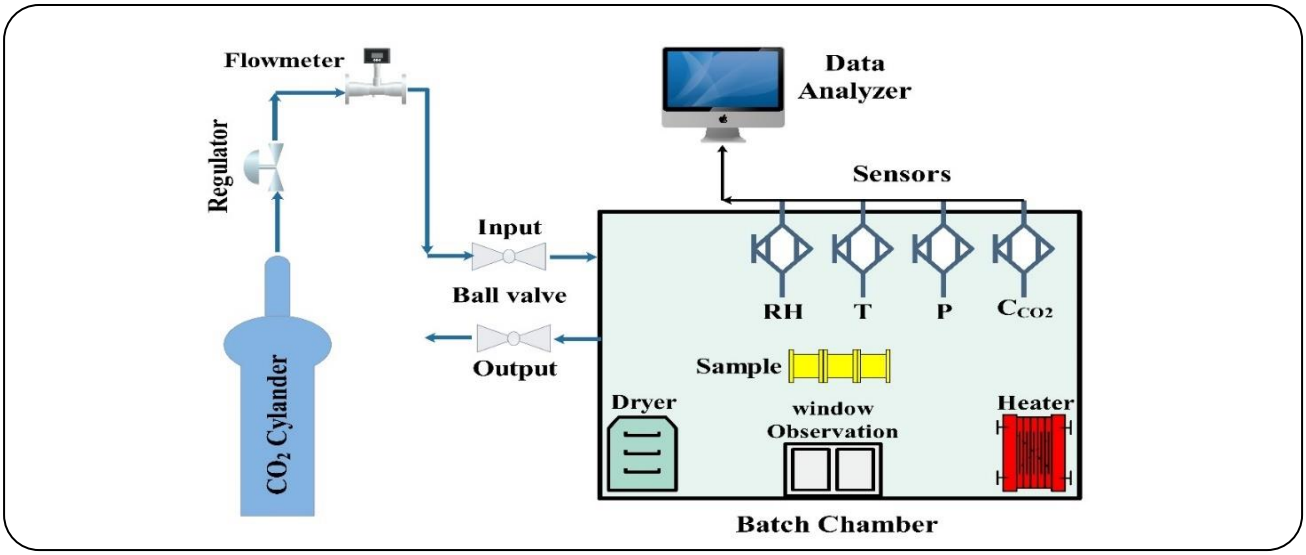

Fig. 3: The schematic view of the experimental adsorption process set-up.

Therefore, to determine the capacity and percentage of CO_2 adsorption in KO_2 nanocomposites as adsorbents, the laboratory set-up shown in Fig. 3 was designed and used. The device consisted of a Plexiglass batch chamber with dimensions 60×60×60 cm and a total volume of 216 cm^3, pure carbon dioxide gas capsule, heater, pressure gauge, regulator, and ball valves. The reactor door was designed in such a way that the environment was completely isolated and gas waste during the process was minimized. The chamber was equipped with carbon dioxide, temperature, and humidity sensors, a barometer, a humidifier, and two valves for the entrance and exit of carbon dioxide gas. The adsorbents were weighed using a digital balance and then was placed inside a cell in the reactor chamber. This chamber was connected to a panel for displaying the temperature and internal pressure during the process. At the beginning of each test, the temperature and humidity are adjusted to the desired values. Initial CO_2 concentration was regulated by entering pure CO_2 gas into the reactor with a pressure gauge and the valve connected to the reactor. Adsorption experiments were carried out for an hour and the equilibrium concentration of carbon dioxide was recorded at any time.

The adsorption capacity of the adsorbent was calculated with Eq. (9) [36]:

$$q_e = \frac{(C_0 - C_e)V}{m} \quad (9)$$

The adsorption percentage of the adsorbent was calculated using Eq. (10) [36].

$$\text{Adsorption}(\%) = \frac{(C_0 - C_e)}{C_0} \times 100 \quad (10)$$

Where C_0 is the initial concentration (mg/L), C_e is the equilibrium concentration (mg/L), V is the volume of the reactor (L), m is the mass of the adsorbent (g), and q_e is the adsorption capacity (mg/g). The fitting degree of kinetic models with the experimental data can be analyzed by correlation coefficient (R^2) (see Eq. (11)). This value may vary from 0 to 1.

$$R^2 = \frac{\left(q_{e,meas} - \overline{q_{e,calc}}\right)^2}{\sum\left(q_{e,meas} - \overline{q_{e,calc}}\right)^2 + \left(q_{e,meas} - q_{e,calc}\right)^2} \quad (11)$$

Where $q_{e,\,meas}$ is the measured adsorption capacity and $q_{e,\,calc}$ is the adsorption capacity obtained from the isotherm and kinetic model and $\overline{q_{e,calc}}$ is the mean of $q_{e,\,calc}$ [24].

Thermodynamic studies can help us to better understand the adsorption process and thus apply measures to increase adsorption efficiency. By examining the changes in the rate of adsorption in terms of temperature, one can comment on the nature of the reaction (whether it is endothermic or exothermic) [37]. By examining the effects of temperature, the optimum temperature required to achieve maximum absorption and recovery can be obtained, and then the absorption constants and equilibrium constants can be calculated from the slope of the curves. It can also be found that physical adsorption takes place on a solid bed with a chemical or physical bond. The adsorption

process occurs at a lower temperature than is economically affordable [23].

RESULTS AND DISCUSSION

Selection of the materials for the in-situ synthesis reactions

Reaction 1 can proceed by mixing KOH (90 wt. %) and H_2O_2 (50 wt. %) at various concentrations. The utilization of a high concentration H_2O_2 solution will elevate the reaction temperature, accelerate the decomposition rate, and thus lower the KO_2 purity. On the other hand, the concentrations of less than 40 wt. % were found to be useless. This reaction is strongly exothermic under normal conditions. Hence, it is required to chill the reaction flask or to feature a stabilizer. The latter is the preferred choice because of the lack of any need for power consumption. The suitable stabilizer should keep oxygen available in the alkaline solution for an extended period and also be appropriate in terms of toxicity, thermal stability, and chemical resistance to atomic oxygen. Magnesium sulfate was considered a suitable stabilizer [38]. The dependence of the influence of the content of peroxide oxygen in the initial solution of potassium peroxide peroxo hydrate on the purity of the obtained KO_2 on the matrix was investigated. The content of KO_2 and alkali KOH was analyzed in the finished product. The experimental results are shown in Fig. 4. As follows from the data obtained, with a decrease in the concentration of peroxide oxygen in the initial alkaline solution of hydrogen peroxide, a decrease in the content of KO_2 in the regenerative product and an increase in the content of alkali are observed.

An increase in the concentration of alkali in the solution and dry product after synthesis had several negative aspects. This result in the decomposition of the KO_2 formed during the drying process during heating; an excessive amount of alkali contributes to an increase in the water vapor pressure over the dried product and KO_2 here acts as an absorbent agent and loses active oxygen.

Magnesium sulfate is more suitable because of the stabilizer[38]. Additionally, $MgSO_4$ doesn't affect the qualitative composition of the ultimate product, is reasonable and simply available, and products didn't decompose either. The solution stabilized with $MgSO_4$ (in the molar ratio $MgSO_4$: H_2O_2 = 1: 750) remains stable at some point at temperatures of up to 25 °C[25].

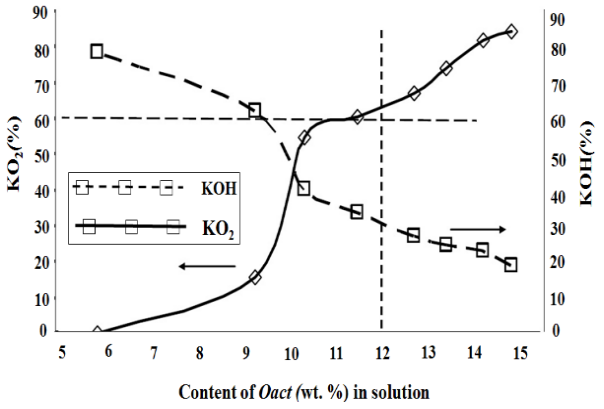

Fig. 4: Dependence of KO_2 and KOH in the regenerative product on the content of peroxide oxygen in the initial solution.

The $MgSO_4$ is available in bulk and neither affects the qualitative composition of the ultimate product nor decomposes the product. The solution stabilized with $MgSO_4$: H_2O_2 molar ratio of 1: 750 remains nearly stable at temperatures of up to 25 °C.

The selection of a matrix for the in-situ synthesis of regenerative porous KO_2 nanocomposite is extremely important because the presence of minute impurities within the solution will cause a quick loss of oxygen. The suitable matrix should be porous, hydrophilic, versatile, thermally stable, non-combustible in touch with active oxygen-containing materials, permeable, inert, immune to alkaline, and oxidizing agents, and possess an oxygen index of ~100%. Considering these attributes, the glass structures including mat, needle mat, and wool were compared through a series of separate preliminary experiments. The alkali resistance of fiberglass matrixes had evaluated. To do this, small pieces of samples were placed in closed bottles filled with an alkaline solution of hydrogen peroxide, kept in a draft at room temperature, periodically observed, and noted changes in the samples visually. During the first day, the appearance of air bubbles (oxygen) was observed simultaneously in all weighing bottles. This is due to the decomposition of hydrogen peroxide in the presence of alkali after 2 hours. Finally, the glass wool was selected as the base matrix and used in all tests because of high porosity, hydrophilicity, heat resistance, and terminal flexibility. This white matrix with unidirectional weave patterns has an aerial weight of ~200-880 g/m^2, density 2.55 g/cm^3, and fabric thickness ~0.16-0.34 mm.

Table 1: Different experimental conditions for studying the effect of parameters on the in-situ synthesis of KO_2 nanocomposite based on the Taguchi experiment design $L_{18}(3^5)$ orthogonal array matrix.

Experiment No	Factors					Response, O_{act} (wt. %)	Product (g)
	A	B	C	D	E		
	Air temperature (°C)	Aeration Time (min)	Aeration distance from surface (cm)	Flow rate of aeration (L/min)	Molar ratio of intermediate solution (%)		
1	1	1	1	1	1	30.93	0.12
2	1	2	2	2	2	36.34	0.15
3	1	3	3	3	3	30.33	0.18
4	2	1	1	2	2	20.14	0.12
5	2	2	2	3	3	18.56	0.12
6	2	3	3	1	1	23.30	0.10
7	3	1	2	1	3	25.43	0.16
8	3	2	3	2	1	11.11	0.14
9	3	3	1	3	2	13.50	0.18
10	1	1	3	3	2	26.03	0.17
11	1	2	1	1	3	27.11	0.16
12	1	3	2	2	1	38.37	0.11
13	2	1	2	3	1	35.71	0.14
14	2	2	3	1	2	24.78	0.12
15	2	3	1	2	3	31.36	0.14
16	3	1	3	2	3	28.11	0.13
17	3	2	1	3	1	15.19	0.16
18	3	3	2	1	2	18.25	0.19

In–situ synthesis of the KO_2 nanocomposite

All the synthesis experiments were performed by the same strategy following the proposed Taguchi design. The response was presented as the average percentage of active oxygen, Table1. The amount of ultimate product formed on the matrix as a control response is additionally measured and presented in the last column of Table 1.

Due to the heat sensitivity of KO_2 powder, its quality and purity are highly influenced by the temperature of the synthesis process [39]. The rate of decomposition of the obtained powder increases under high-temperature synthesis conditions. In general, reducing the amount of KO_2 in the final product reduces the capacity of active oxygen. To prevent this phenomenon, researchers are seeking low-temperature synthesis methods. The review of the references shows that reducing the reaction temperature from 210 to 20 °C improves the process efficiency from 20 to 90% by weight compared to the amount of KO_2 powder obtained [40, 41]. Therefore, lowering the synthesis temperature using the various techniques leads to a higher quantity and quality of KO_2 as a product.

The average effects of the factors and interactions at the appointed levels on Oact (wt. %) have been presented in Table 2. The difference between the average value of each factor at levels 2 and 1 indicates the relative influence of each factor. The more significant the difference, the stronger the impact. In Table 2, the sign of the difference (+ or −) indicates whether the change from level 1 to level 2 or 3 increase or decrease the result. Based on these data, it can be observed that the temperature of the air, aeration distance from the surface, and aeration time for aeration have a more influential effect than the other factors.

Table 2: Main effects of the factors and interactions at the assigned levels on active oxygen in wt. %.

Designation	Explanation	Level 1	Level 2	Level 3	L2 - L1
A	Temperature of air (°C)	31.851	25.268	19.193	-6.583
B	Time for aeration (min)	27.674	22.398	26.239	-5.276
C	Aeration distance from surface (cm)	23.653	29.433	23.226	5.78
D	Flow rate of aeration (L/min)	25.456	26.481	24.375	1.025
E	Molar ratio of intermediate solution (%)	26.151	24.934	22.226	-1.217

The least impact was noticed with the molar ratio of the intermediate solution and flow rate of aeration with the assigned levels.

The interactions of various factors show that the flow rate of aeration (D) versus the molar ratio of intermediate solution (E) has the highest severity index percentage (SI), ~69.81%. Similarly, the severity index percentage for the temperature of the air (A) versus the molar ratio of intermediate solution (E) was of the smallest SI, only 7.04%. These results suggest that the influence of one factor on the active oxygen content was dependent on the condition of the other factors in optimizing the process parameters of the in-situ synthesis.

Fig. 5 shows the O_{act} (wt. %) profiles for all levels of five factors. It can be observed that the highest percentage of active oxygen is achieved at level 1 of parameters A, B, and E, and level 2 of parameters C and D. From one experiment to the next, the levels of several control factors must be changed. This poses a considerable amount of difficulty to seek out a historical record with an equivalent control factor level. Failure to set the level of a factor correctly could destroy the precious property orthogonally and lead to wrong conclusions.

The percentage contribution of each factor and the results of the S/N-variance analyses followed by Fisher's test were presented in Table 3. The percent value in the last column of the ANOVA table indicates the influence of each factor. The percent (%) was defined as the significant rate of the process parameters on the in-situ synthesis. The temperature of hot air was the foremost effective factor on O_{act} (wt. %) in air resuscitation porous KO_2 nanocomposite. It can be seen from the results that physical factors such as the temperature of air (A) and aeration distance from the surface (C) play more significant roles in the product formation than the other selected parameters and their levels.

The essential criterion in the Taguchi method for analyzing experimental data is signal/noise ratios. In this study, the S/N ratio should have a maximum value to be considered as the optimum. A higher SNR indicates a higher percentage of active oxygen.

Accordingly, it can be observed that the slope of the curve (Fig. 6), the inter-surface variations in temperature of the air, and aeration distance from the surface are steeper than the others so that an increase or decrease in the amount of these parameters over the other ones can cause significant changes in the performance of the air regenerative KO_2 nanocomposite. The desired content of O_{act} (wt. %) can be provided by controlling the temperature as the most prominent physical parameter.

The Taguchi method was used to determine the optimum operating conditions. In contrast, the interaction between the in-situ synthesis parameters was established by ANOVA analysis. The optimum levels of the parameters were identified to form the highest performance in the predicted results by the Taguchi experimental design (Table 4). The software also predicts the performance of air regenerative nanocomposites, consistent with the experimental results. The anticipated conditions for in-situ synthesis were prepared and verified in the laboratory (Table 4).

Characterization of the optimal KO_2 nanocomposite

XRD analysis

The XRD pattern of the optimum in-situ synthesized nanocrystals has been shown in Fig. 7. The optimum sample was fully authenticated by the XRD pattern and exhibited good crystallinity confirming that the condition of in-situ synthesis has been suitable for the crystallization process. The sample shows a predominant KO_2 component and minimal amounts of KOH; H_2O. The NaO_2 and SiO_2 phases have shown low-intensity peaks and an almost amorphous structure. The phase identified for potassium hydroxide

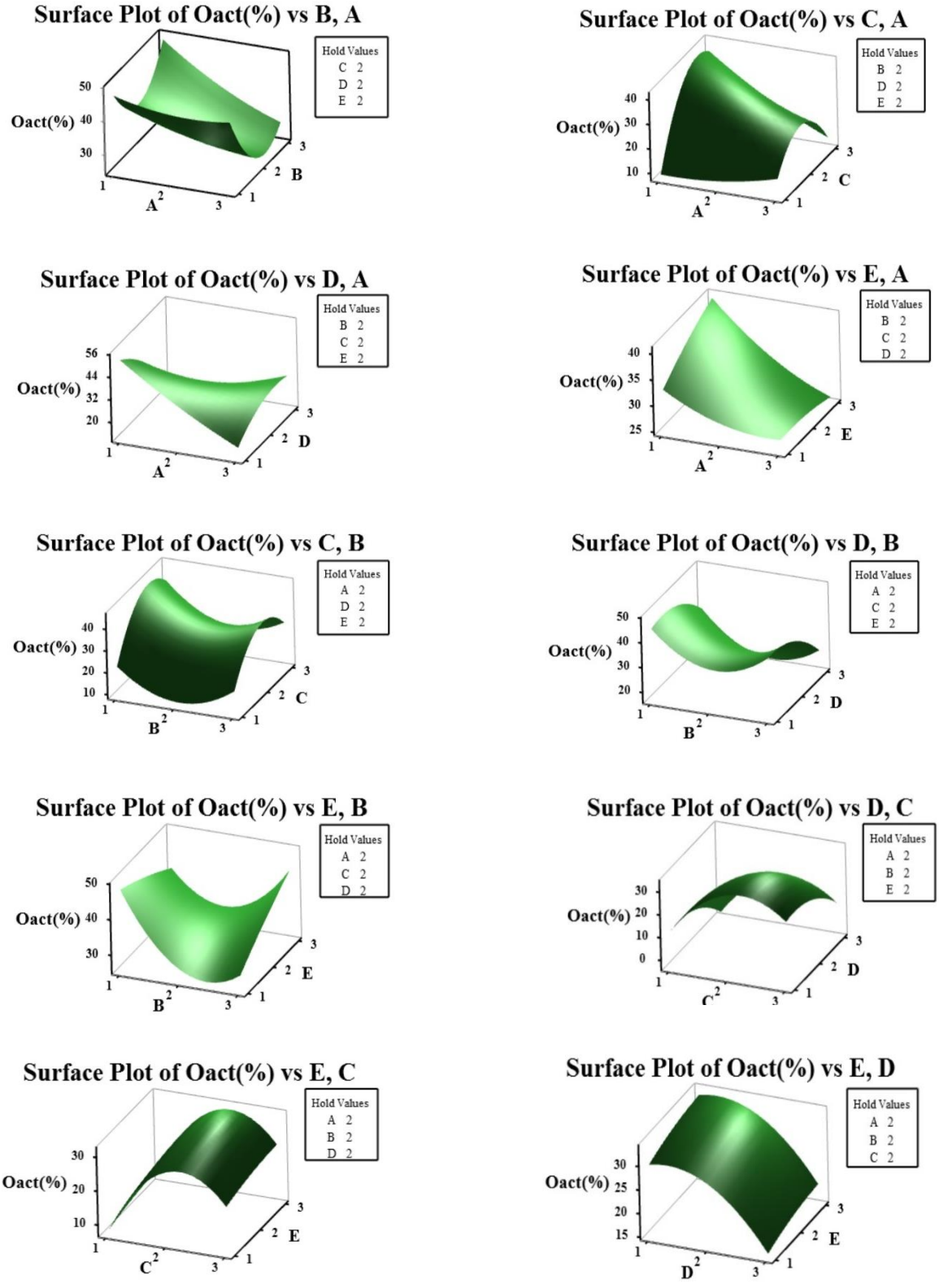

Fig. 5: The 3D response surface plots of the Oact (wt. %) as a function of two factors at fixed values of other ones.

Table 3: Analysis of variance (ANOVA) for Oact (wt. %) using a factorial experimental design.

Factor	Degree of freedom	Sum of Squares	Variance	F-Ratio	Pure Sum	Percent
A	2	480.958	240.479	8	420.843	44.625
B	2	89.32	44.66	1.485	29.205	3.096
C	2	144.227	72.113	2.399	84.112	8.919
D	2	13.316	6.658	0.221	0	0
E	2	4.481	2.42	0.08	0	0
Other/Error	7	210.401	30.057			43.36
Total	17	943.065				100%

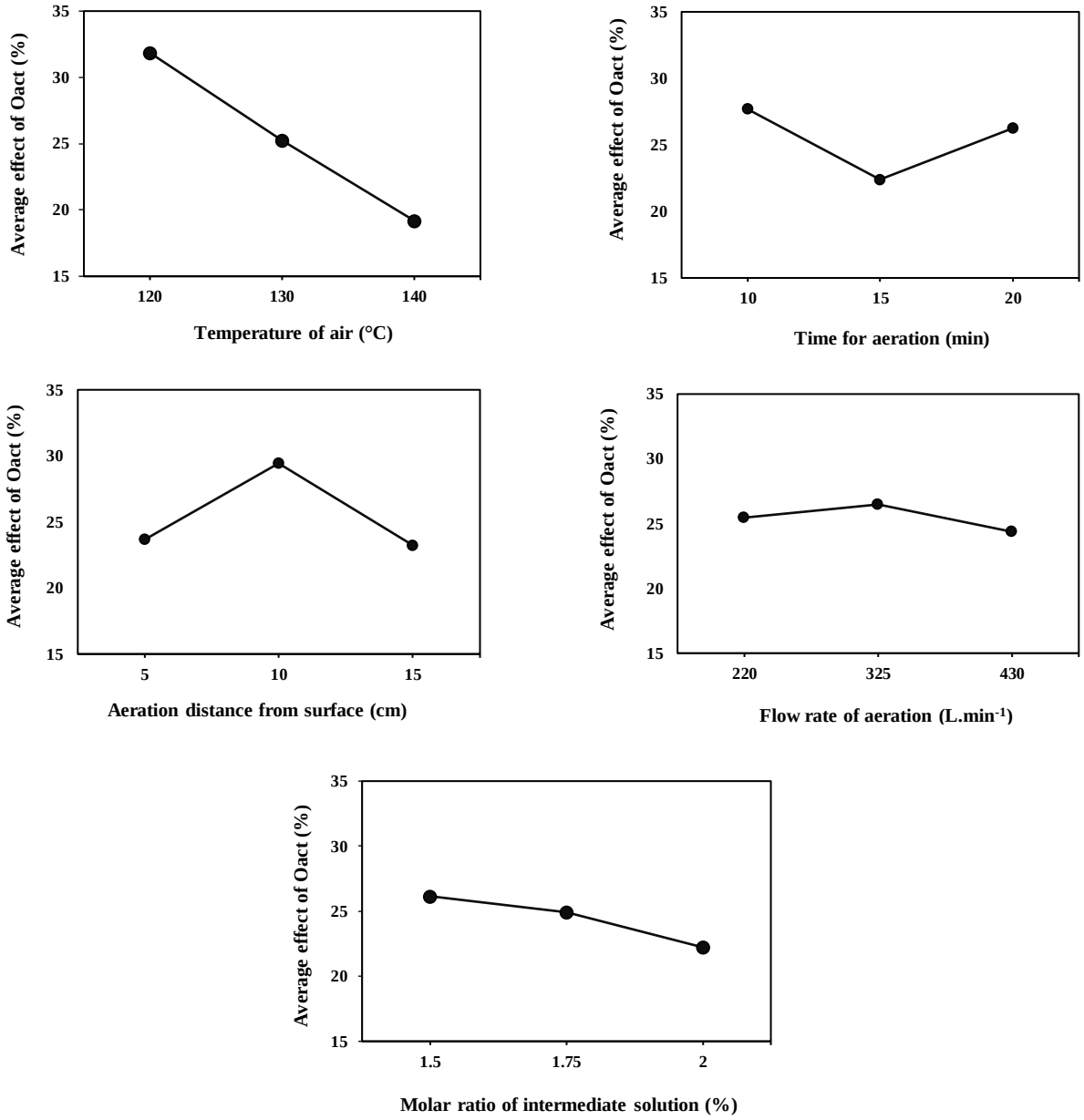

Fig. 6: Effects of each factor at specific levels on the S/N ratios based on Taguchi experimental design. The vertical axis shows the average signal-to-noise ratio as calculated by Eq. 5.

Table 4: The Taguchi design model for optimum operating conditions of in-situ synthesis along with the predicted and measured value of active oxygen as the response.

Factor	Level	Value	Contribution	Predicted O_{act} (wt. %)	Measured O_{act} (wt. %)
Temperature of air (°C)	1	120	6.413	39.838	39.53
Time for aeration (min)	1	10	2.237		
Aeration distance from surface (cm)	2	10	3.995		
Flow rate of aeration (L/min)	2	325	1.043		
Molar ratio of intermediate solution (%)	1	1.5	0.713		

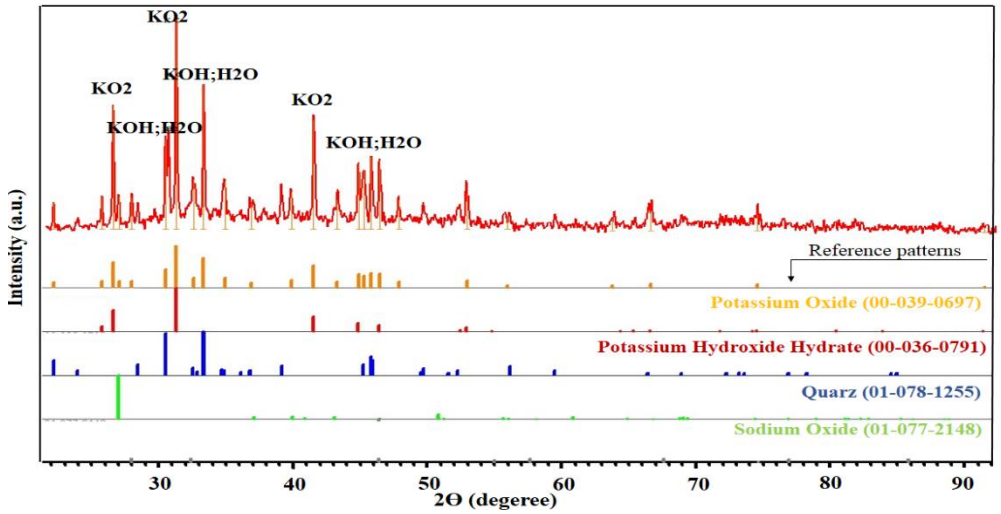

Fig. 7: XRD patterns of in-situ synthesized KO_2 nanocrystals under optimum physicochemical conditions.

as the impurity of the process is due to KO_2 synthesis under air pressure and in the presence of CO_2 and moisture. This problem was minimized by optimizing the synthesis conditions of the final product on the fiberglass bed. The sodium oxide phase is present due to impurities in the used potassium hydroxide as the raw material. The amount of quartz observed in the pattern is related to the silica structure of the fiberglass bed. Considering the standard JCPDS pattern (00-039-0697) of KO_2 with characteristic peaks at $2\Theta = 31.31, 26.16, 41.52, 46.43, 44.86$, and 52.97 [42], the formation of the desired crystals were confirmed. The mean crystal size was also calculated using the peaks in the XRD patterns according to the Debye–Scherrer equation [43]:

$$D = K\frac{\lambda}{\beta\cos\theta} \qquad (12)$$

Where, K is the shape factor equal to 0.94 for spherical particles, λ is the wavelength of Cu K_α radiation equal to 0.1540598 nm, β represents the halfwidth of each diffraction peak, and θ stands for the Bragg angle. According to this relationship, the nanocrystals have a mean diameter of 35±5 nm.

FESEM-EDX analysis

Fig. 8(I) presents the FESEM micrographs of the plate surface at different magnifications. It shows that the monolayers of highly dispersed KO_2 were formed on the highly porous matrix of ultrathin fiberglass. In part (a) of Fig. 8(I), the in-situ synthesized porous KO_2 nanocomposites are visible on the fiberglass matrix. In part (b), the KO_2 nanocrystals have appeared in irregular shapes and agglomerated in some places, consistent with other findings in the literature [44]. As shown in part (d), the minimum and maximum particle sizes were about 15±5 and 35±5 nm, respectively. These results are in good agreement with the results of the XRD analysis. The obtained elemental map by EDX also confirms

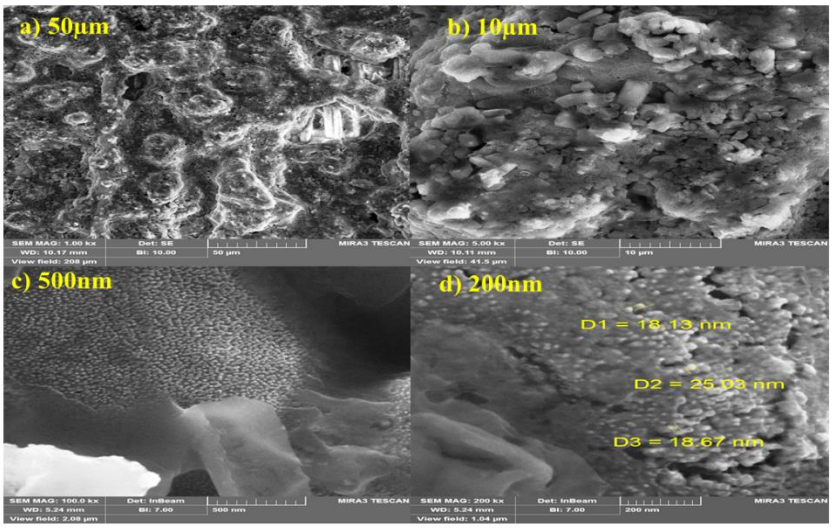

(I)

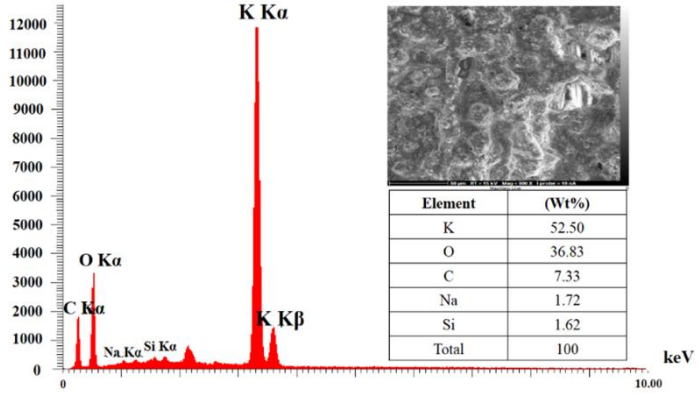

(II)

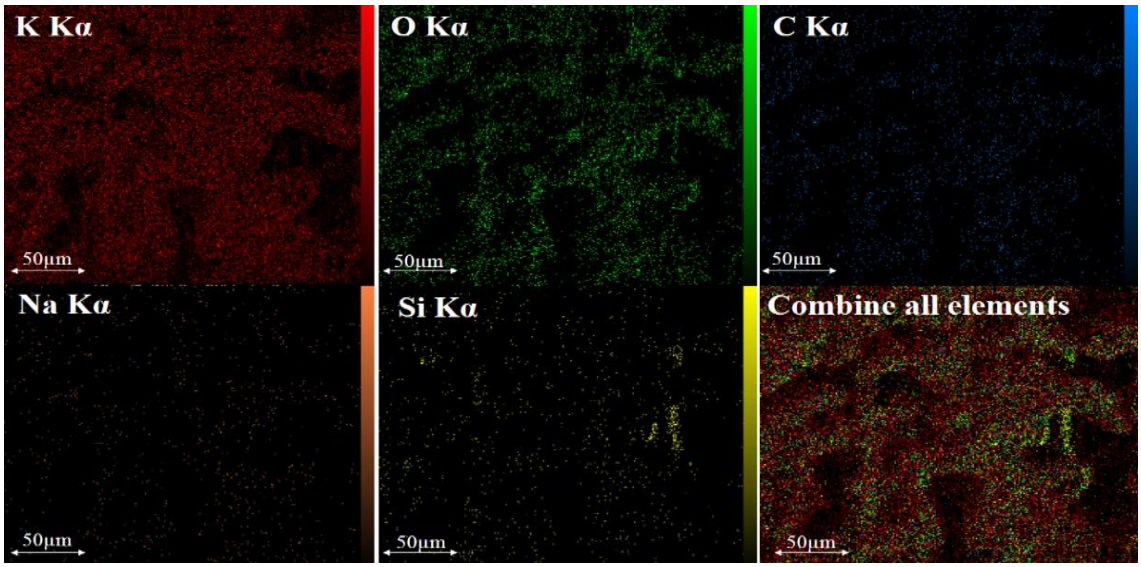

(III)

Fig. 8: (I) FE-SEM micrographs of optimum KO_2 nanocrystals, (II) the EDX plot of the specimen, and (III) the elemental map of the detected elements by EDX.

the formation of KO_2 nanocomposites on the matrix, Fig. 8(II). As shown in Fig. 8(II), the EDX plot reveal the presence of the following elements: K = 52.50 wt%, O = 36.83 wt%, C =7.33 wt%, Na = 1.72 wt%, Si = 1.62 wt%. This analysis indicates that the sample is composed of KO_2 and the other peaks appear from the structure of the fiberglass matrix. The result shows the high concentrate grade of KO_2 and in-situ synthesis of pure nanocrystals on the matrix. The dot mapping images in Fig. 8(III) show a nearly uniform distribution of the K and O elements for all samples.

Surface area and pore size distribution

The surface area was determined based on the nitrogen adsorption/desorption isotherms and the equation of Brunauer, Emmett, and Teller (BET) for multilayer adsorption[45]. The pore volume was calculated based on the amount of liquid nitrogen adsorbed at P/P_0=0.990 (where P is the equilibrium pressure and P_0 is the saturation pressure of the adsorbate at the measurement temperature)[46]. The equilibrium time of 30 min was considered for the adsorption process. The adsorption and desorption isotherms of nitrogen of optimum nanocomposite bed before and after the in-situ synthesis KO_2 nanocrystalline process were shown in Fig. 9. As shown in this figure, the structure of the nanocomposite beds and based on the size of the pores of the samples (between 3 and 50 nm), were mesoporous IV-type isotherm and the mesoporous solids according to the IUPAC standard classification[47]. The typical hysteresis between adsorption and desorption was observed. The adsorption/desorption curves of the nanocomposite bed after the process of in-situ synthesis, show that micellar pores were almost filled or blocked by KO_2 nanocrystalline, and there is a small rise at high partial pressure due to capillary condensation in larger pores[48]. The hysteresis between adsorption and desorption curves at the second rise confirms that there is a distribution in pore size at that range. This fact is thoroughly justified in Fig. 8.

The pore size and total volume were calculated based on pore size distributions in the adsorption branches of the isotherms were obtained by using the Barret-Joyner-Halenda (BJH) method and were presented in Fig. 10. The average porosity volume and diameter by the BJH method, before the in-situ synthesis process of KO_2 nanocrystalline, for fiberglass bed were 0.0057535 cm^3/g and 1.21 nm, and for the nanocomposite bed produced,

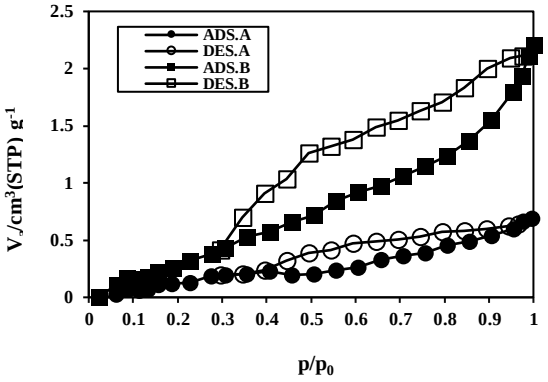

Fig. 9: Nitrogen adsorption and desorption isotherms of optimum nanocomposite bed before and after the in-situ synthesis KO_2 nanocrystalline process.

0.0014182 cm^3/g and 1.21 nm, respectively. A comparison of the geometric surface area to the specific surface areas shows the pores in the beds are approximately filled with synthesized nanocrystals, however, there are still open pores for the penetration of carbon dioxide and water vapor to react and the porosity of the bed is maintained. The quantitative characteristics of the nanocomposite beds are shown in Table 5.

TG analysis

The TG curve (Fig. 11) of the synthesized samples confirms a similar decomposition curve for the supported-mesoporous KO_2 nanocomposite regenerative products to the other powdered KO_2 in literature [14]. Up to a temperature of 100°C, the weight loss was 2–2.5%, which corresponds to the removal of free water. The significant weight loss in the range of 100–250°C in all samples is related to the adsorbed water on the crystal surface.

Kinetics models

The kinetic behavior of the CO_2 adsorption process of optimal KO_2 nanocomposites was studied by five kinetic models offered in Table 6 [49]. The kinetic parameters' values were characterized at a temperature of 25 °C and humidity of 60 % to specify the best kinetic model. On the other hand, comparing kinetic adsorption models linearly extracted from the nonlinear form of Table 6 with experimental data at 25°Cis performed in Fig. 12.

It can be seen from the R^2 values in Table 6 that the first-order and Ritchie second-order models are inefficient for the experimental data of KO_2 nanocomposites, while the Elovich and second-order models are highly

Table 5: Structural features of optimum nanocomposite beds before and after the in-situ synthesis KO_2 nanocrystalline process.

Sample	$a_{s,\ BET}$ (m^2/g)	V_m (cm^3(STP)/ g)	Mean pore diameter (nm)	Total pore volume, p/p_0=0.990, (cm^3/g)
Optimum nanocomposite bed, Before	2.2203	0.5101	9.3186	0.00517
Optimum nanocomposite bed, After	1.2528	0.2878	4.1185	0.00129

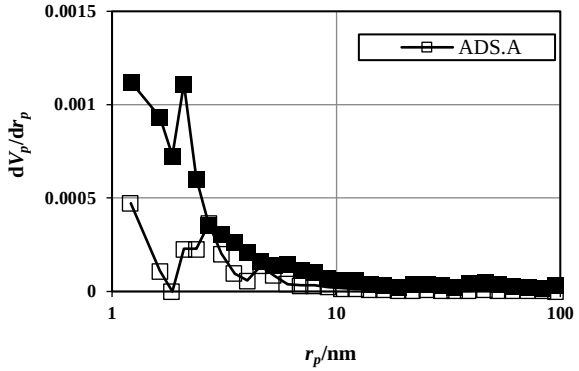

Fig. 10: The BJH particle size distribution (inset) diagram in of optimum nanocomposite beds.

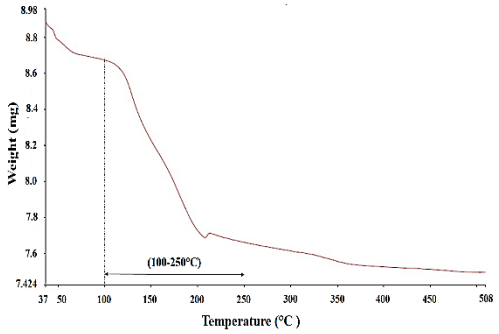

Fig. 11: TGA analysis of the in-situ synthesized nanocrystals in the range of 40 to 550 °C.

compatible. The first-order model shows the reversible interactions between the adsorbent and the adsorbate [50]. In contrast, the second-order model assumes that the interactions between the adsorbate and the adsorbent are due to the strong bonding of the fluid to the adsorbent surface. This model is used when the adsorption process is chemical adsorption.

Elovich model is suitable for defining systems with heterogeneous adsorption surfaces, especially adsorption of gases on solid surfaces [51-53]. Rate controlling or intraparticle diffusion [54, 55] is usually concerned with the transfer of metal ions from the liquid to the adsorbent through the liquid diffusion into the adsorbent particles' pores. The high amount of R^2 in this model is due to the diffusion of gaseous fluid (CO_2) as the adsorbate in the structure of the nanocomposite substrate layers.

Comparing the presented results in Fig. 12 and the correlation coefficients of adsorbent, it can be concluded that the Elovich model is better than other models with a value of R^2 of 0.9895.

The compatibility of this model with the current trend is due to the heterogeneous mechanism of CO_2 adsorption on the optimal KO_2 nanocomposites. This indicates that the adsorbent surface is not uniform for CO_2 adsorption and the active sites for adsorption are not constant. Therefore, CO_2 adsorption in optimal KO_2 nanocomposites can be described as a combination of chemical and physical adsorption. Therefore, it can be described the CO_2 adsorption on the optimal KO_2 nanocomposites as a combination of chemical and physical adsorption [60]. On the other hand, the results of the second-order kinetic model show that the value of q_e obtained from this model is close to the experimental q_e. Also, after the Elovich model, this model is in good agreement with the experimental data. Because the adsorbent is optimized during in situ synthesis, the second-order model illustrates well the chemical interactions in the modified adsorbent.

Thermodynamic

Determination of thermodynamic parameters of adsorption including entropy change (ΔS°), enthalpy change (ΔH°), and Gibbs free energy change (ΔG°), is important to describe the adsorption processes. These parameters can be computed using Eq. (18)[61]:

$$\mathrm{Lnk_d} = \frac{\Delta S^\circ}{R} = -\frac{\Delta H^\circ}{RT} \tag{18}$$

ΔS° is standard entropy, ΔH° is standard enthalpy, T is the absolute temperature, and R is the gas constant. k_d is the distribution coefficient, calculated using Eq. (19)[36]:

$$\mathrm{k_d} = \frac{C_{CO_2}^{initial} - C_{CO_2}^{final}}{C_{CO_2}^{final}} \times \frac{\upsilon}{\omega} \tag{19}$$

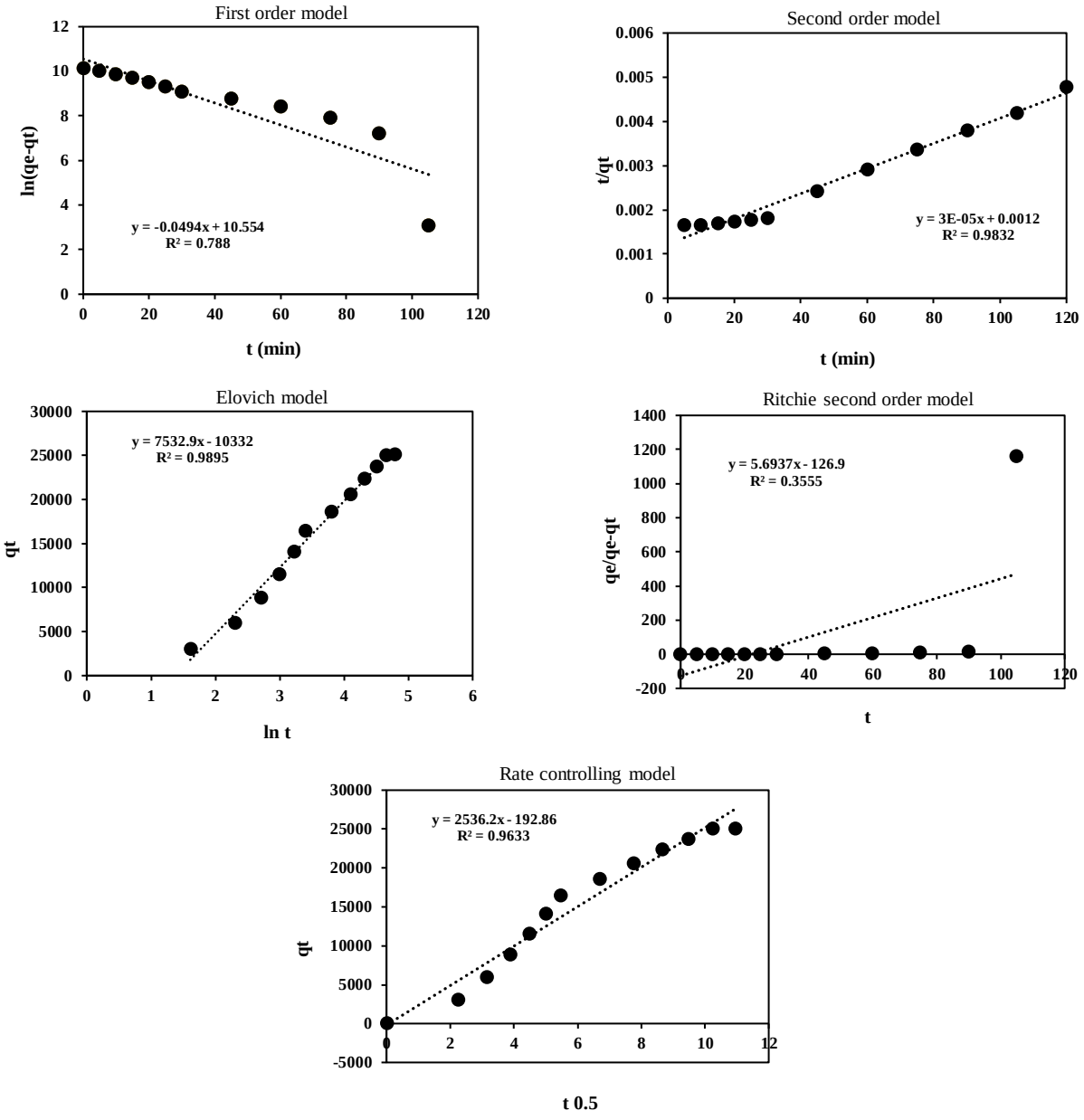

Fig. 12: Kinetic modeling for CO_2 adsorption on optimal KO_2 nanocomposites.

Where $C_{CO2}^{initial}$ is the initial concentration (mg/L), C_{CO2}^{final} is the final concentration (mg/L), m is the mass of adsorbent (g) used and v is the volume (L) of the gas. As shown in Fig. 13, a straight line is obtained by drawing changes of Ln (k_d) versus 1/T. By calculating the slope and y-intercept of the graph, ΔH° and ΔS° can be obtained respectively. In this case, the Gibbs standard energy value can be calculated from Eq. (20)[62]:

$$\Delta G^{\circ} = \Delta H^{\circ} + T\Delta S^{\circ} \quad (20)$$

Fig. 13 shows the values of the distribution coefficient (Kd) decrease by temperature increasing. This indicates that the adsorption process is exothermic. Fig. 14 shows the change in CO_2 adsorption with temperature for KO_2 nanocomposites.

The results of the thermodynamics parameters have been presented in table 7. A negative ΔH ° indicates that the adsorption process is exothermic, and therefore the adsorption rate decreases with increasing temperature. A positive ΔS° indicates an increase in irregularity

Table 6: Parameters of kinetic models of CO_2 adsorption using optimal KO_2 nanocomposites (298.15 K).

Kinetic model	Nonlinear form	Eq.number	Parameter
First order[56]	$q_t = q_e\left(1-\exp\left(-k_1 t\right)\right)$	13	q_e = 38330.45
			K_1 = 0.0494
			R^2 = 0.788
Second order[56]	$q_t = k_2 \cdot q_e^2 \frac{t}{\left(1+k_2 \cdot q_e \cdot t\right)}$	14	$q_e = 3.33*10^4$
			$K_2 = 7.5*10^{-7}$
			R^2 = 0.9832
Elovich[57]	$q_t = \beta \cdot \log\left(\alpha \cdot \beta\right) + \beta \cdot \log\left(t\right)$	15	$\alpha = 3.36*10^{-5}$
			β = 7532.9
			R^2 =0.9895
Ritchie second order[58]	$q_t = q_e \frac{q_e}{\left(1+k_2 \cdot t\right)}$	16	q_e = 25077.6
			K_2 = 5.6937
			R^2 = 0.3555
Rate controlling[59]	$q_t = k_{id} \cdot t^{0.5}$	17	k_{id} = 2536.2
			R^2 = 0.9633

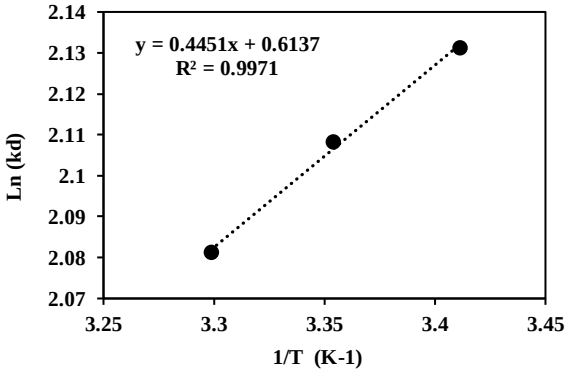

Fig. 13: The plot of Ln k_d vs. 1/T for adsorption of CO_2 on optimal KO_2 nanocomposites.

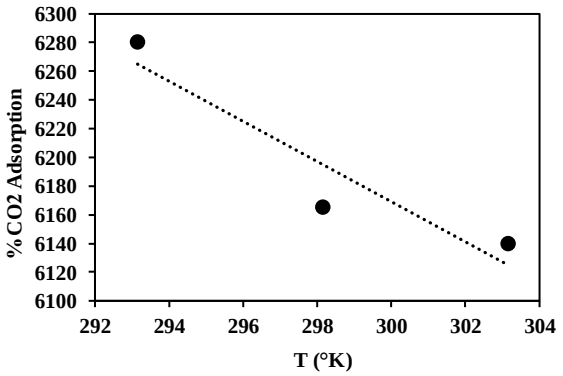

Fig. 14: Variation of CO_2 adsorption percentage with temperature for the KO_2 nanocomposites.

in the adsorption process. It can be due to the production of by-products at the surface of the adsorbent sites, which ultimately leads to irregularities in the structure and final deformation. Enthalpy change is assumed to be constant for examining $\Delta G°$ values at different temperatures. The negative $\Delta G°$ at all temperatures demonstrates that the adsorption process is spontaneous. As the results show, the value of $\Delta G°$ decreases with increasing temperature, which indicates a higher adsorption capacity at lower temperatures[23, 63].

CONCLUSIONS

In this study, the Taguchi method based on the L_{18} orthogonal array was successfully applied to understand the effect of physicochemical parameters involved in situ synthesis of KO_2 nanocomposites to improve O_2 production (active oxygen content) and CO_2 adsorption capacity as the chemical lung. The present research used an alkaline solution of hydrogen peroxide with fiberglass as a matrix by drying at atmospheric pressure with heated air to produce KO_2 nanocrystals fixed on the fiberglass.

Table 7: Thermodynamics parameters of CO_2 adsorption by KO_2 nanocomposites.

ΔH° (kJ/mol)	ΔS° (kJ/mol.K)	ΔG°(kJ/mol)		
		293.15	298.15	303.15
-3.7005	0.0051	-5.1963	-5.2218	-5.2473

The optimal KO_2 nanocomposites were synthesized, characterized, and evaluated for the CO_2 adsorption process. The analysis of variance (ANOVA) with Fisher's test revealed that the most significant rate of 44.62 %, at $p \leq 0.05$ on the response was exerted by the temperature of hot air. The optimal O_{act} (wt. %) was 39.53 and verified experimentally. The XRD pattern and TGA decomposition curves of the optimum sample confirmed the form of KO_2 nanocrystals as a major phase on the matrix. The FESEM and EDX analysis showed the uniform distribution of the KO_2 nanocrystals both in pores and on the surface of the fiberglass matrix. The KO_2 nanocrystals were present in the form of small spherical or semispherical grains with diameters of 10–40 nm. The BET specific surface area of KO_2 nanocomposite was measured at about 1.2528 m^2/g and they have a mesoporous solid structure. By kinetic and thermodynamic modeling, the comparison between predicted and empirical data, the CO_2 adsorption process behavior was found to be close to the ideal model. Kinetic studies have been carried out using different kinetic models and the Elovich model is more consistent with experimental data, showing that the heterogeneous adsorption mechanism of CO_2 on optimal KO_2 nanocomposites is valid. Thermodynamic results confirm that the reaction is spontaneous in nature and exothermic. Finally, our data for the first time reveal the way to achieve a modified design for scale-up of the in-situ synthesis process to produce optimal KO_2 nanocomposite. In addition, it can be concluded that the optimal mesoporous KO_2 nanocomposites in this way by maintaining the maximum content of active oxygen have emerged as a potential new adsorbent for CO_2 adsorption from the air and can be used as a chemical lung directly in the air revitalization systems.

Acknowledgments

The authors are grateful for the financial support of Malek Ashtar University of Technology (Tehran, Iran). This work did not receive any specific grant. Proofreading and editing by Hamyarapply (Tehran, Iran) are greatly acknowledged.

Received: Oct. 26, 2021 ; Accepted: Jan. 31, 2022

REFERENCES

[1] Kim J.H., Park Y., Jeong S.K., CO_2 Conversion to O_2 by Chemical Lung in the Presence of Potassium Superoxide in the Silicone Polymer Matrix, *Korean Journal of Chemical Engineering*, **27(1)**: 320-323 (2010).

[2] Stull J., White M., Air Revitalization Compounds: A Literature Survey, *Toxicological & Environmental Chemistry*, **10(2)**: 133-155 (1985).

[3] Wang S., Zhang T., Jin L., Revitalization of Air Using a Potassium Superoxide Plate in Hypoxic Space: Performance and Kinetic Model under Natural Convection Conditions, *Indoor and Built Environment*, **28(5)**: 599-610 (2019).

[4] Mulloth L., Finn J., Air Quality Systems for Related Enclosed Spaces: Spacecraft Air, *Hdb. Env. Chem.*, **4**: 383-404 (2005).

[5] Ray C., Ogle K., Tipps R., Carrasquillo R., Wieland P., The Space Station Air Revitalization Subsystem Design Concept, *SAE Transactions*, **96**: 508-520 (1987).

[6] Chegeni A., Babaeipour V., Fathollahi M., Hosseini S.G., Development of a New Formulation of Air Revitalization Tablets in Closed Atmospheres Using the Taguchi Statistical Method, *Inter. Jour. Envir. Sci. Techn.*, **19**: 4289–4304 (2022).

[7] Zhdanov D., Ul'yanova M., Ferapontov Y.A., A Study of the Kinetics of Synthesis of Potassium Superoxide from an Alkaline Solution of Hydrogen Peroxide, *Russian Journal of Applied Chemistry*, **78(2)**: 184-187 (2005).

[8] Holquist J.B., Klaus D.M., Graf J.C., Characterization of Potassium Superoxide and a Novel Packed Bed Configuration for Closed Environment Air Revitalization", *44th International Conference on Environmental Systems* (2014).

[9] Holquist J., Koenig P., Tozer S., Wiliams A.A., Kalus D.M., Stodiek L., Niederwieser T., Olthoff C.T., Hohen A., "Atmosphere Regeneration to enable Life Support for the Transport of Rodents to and from the ISS-Design Trades and Test Results", *43rd International Conference on Environmental Systems*, 3461 (2013).

[10] Karelin A., Gladyshev N., Gladysheva T., Raman Spectroscopy Data on the Phase Transition of KO_2 Mixed with KOH on a Glass Fiber Matrix, *Russian Journal of Inorganic Chemistry*, **59(4)**: 360-367 (2014).

[11] Gladysheva T., Gladyshev N., Dvoretsky S., "Nanocrystalline Regenerative Product," *Synthesis. Properties. Implementation. Moscow, Spektr.(Rus.)*, (2014).

[12] Gladysheva T., Gladyshev N., Plotnikov M.Y., Dorokhov R., Dvoretskii S., Karelin A., Kinetics of Carbon Dioxide Chemisorption and Oxygen Release Under Static Conditions by Nanocrystalline KO_2 Deposited on a Fiber-Glass Matrix, *Russian Journal of Applied Chemistry*, **88(6)**: 1015-1019 (2015).

[13] Mas J., Argudo M., Labanda J., Llorens J., "Mass and Volume Efficient CO_2 Removal and O_2 Generation System", SAE Technical Paper 0148-7191, (2007).

[14] T. Gladysheva, N. Gladyshev, and S. Dvoretsky, Advanced Composite Material for Air Regeneration Systems of Individual and Collective Protection, *Advanced Materials & Technologies*, **1**: 44-55 (2016).

[15] Reinsberg P.H., Koellisch A., Bawol P.P., Baltruschat H., $K–O_2$ Electrochemistry: Achieving Highly Reversible Peroxide Formation, *Physical chemistry Chemical Physics*, **21(8)**: 4286-4294 (2019).

[16] Ferapontov Y.A., Ul'yanova M., Sazhneva T., Kinetics and Mechanism of Decomposition of Peroxide Compounds in the Liquid Phase of the KOH-H_2 O_2-H_2O System in Vessels Made of Various Materials," *Russian Journal of Applied Chemistry*, **82(5)**: 826-831 (2009).

[17] Jia Y., Liu Y., Wang S., Reaction Characteristics of Oxygen Generation from Plate-Like Potassium Superoxide within a Confined Space, *Journal of Advanced Oxidation Technologies*, **20(1)**: (2017).

[18] Alem-Rajabif A., Lai F., EHD-Enhanced Drying of Partially Wetted Glass Beads, *Drying Technology*, **23(3)**: 597-609 (2005).

[19] Seyfi R., Babaeipour V., Mofid M.R., Kahaki F.A., Expression and Production of the Recombinant Scorpion as a Potassium Channel Blocker Protein in Escherichia Coli, *Biotechnology and Applied Biochemistry*, **66(1)**: 119-129 (2019).

[20] Babaeipour V., Bagherniya M., Soleimani A., Optimization of Bacterial Nano-Cellulose Production in Bench-Scale Rotating Biological Contact Bioreactor by Response Surface Methodology, *Iranian Journal of Chemistry and Chemical Engineering (IJCCE)*, **40(2)**: 407-416 (2021).

[21] Chegeni A., Babaeipour V., Fathollahi M., Hosseini S.G., Modeling of CO2 Adsorption Isotherms, Kinetics and Thermodynamics Equilibrium, and the Brunauer− Emmett−Teller Analysis onto KO_2 Pellets, *Journal of Cluster Science*, **33**: 2167-2178 (2022).

[22] Saha D., Deng S., Adsorption Equilibrium and Kinetics of CO_2, CH_4, N_2O, and NH3 on Ordered Mesoporous Carbon, *Journal of Colloid and Interface Science*,**345(2)**: 402-409 (2010).

[23] Cui M., Jang M., Cho S.H., Khim J., Kinetic and Thermodynamic Studies of the Adsorption of Heavy Metals on to a New Adsorbent: Coal Mine Drainage Sludge, *Environmental Technology*, **31(11)**: 1203-1211 (2010).

[24] Zheng H., Liu D., Zheng Y., Liang S., Liu Z., Sorption Isotherm and Kinetic Modeling of Aniline on Cr-Bentonite, *Journal of Hazardous Materials*, **167(1-3)**: 141-147 (2009).

[25] Ferapontov Y. A., Zhdanov D., Ul'yanova M., Physicochemical Properties of KOH-H_2O_2-H_2O Solutions, *Russian Journal of Applied Chemistry*, **80(7)**: 1045-1047 (2007).

[26] Allen A., Anderson M., Mattson B., The Remarkable Chemistry of Potassium Dioxide (1–). Two Microscale Classroom Demonstrations, *Journal of Chemical Education*, **86(11)**: 1286 (2009).

[27] Gao N., Jin L., Hu H., Huang X., Zhou L., Fan L., Potassium Superoxide Oxygen Generation Rate and Carbon Dioxide Absorption Rate in Coal Mine Refuge Chambers, *International Journal of Mining Science And Technology*, **25(1)**: 151-155 (2015).

[28] Piramoon S., Aberoomand Azar P., Saber Tehrani M., Mohamadi Azar S., Optimization of Solar-Photocatalytic Degradation of Polychlorinated Biphenyls using Photocatalyst (Nd/Pd/TiO_2) by Taguchi Technique and Detection by Solid Phase Nano Extraction, *Iranian Journal of Chemistry and Chemical Engineering (IJCCE)*, **40(5)**: 1541-1553 (2021).

[29] Yang Y.-S., Huang W., A Grey-Fuzzy Taguchi Approach for Optimizing Multi-Objective Properties of Zirconium-Containing Diamond-Like Carbon Coatings, *Expert Systems with Applications*, **39(1)**: 743-750 (2012).

[30] Ramavandi B., Asgari G., Faradmal J., Sahebi S., Roshani B.,"Abatement of Cr (VI) from Wastewater Using a New Adsorbent, Cantaloupe Peel: Taguchi L 16 Orthogonal Array Optimization, *Korean Journal of Chemical Engineering*, **31(12)**, 2207-2214 (2014).

[31] Gopinath S., Devan P., Optimization and Prediction of Reaction Parameters of Plastic Pyrolysis oil Production Using Taguchi Method, *Iran. J. Chem. Chem. Eng. (IJCCE)*, **39(2)**: 91-103 (2020).

[32] Zhang S., Shen Y., Shao P., Chen J., Wang L., Kinetics, Thermodynamics, and Mechanism of a Novel Biphasic Solvent for CO2 Capture from Flue Gas, *Environmental Science & Technology*, **52(6)**: 3660-3668 (2018).

[33] Wang L., Yu S., Li Q., Zhang Y., An S., Zhang S., Performance of Sulfolane/DETA Hybrids for CO_2 Absorption: Phase Splitting Behavior, Kinetics and Thermodynamics, *Applied Energy*, **228**: 568-576 (2018).

[34] Ho Y., McKay G., A Comparison of Chemisorption Kinetic Models Applied to Pollutant Removal on Various Sorbents, *Process Safety and Environmental Protection*, **76(4)**: 332-340 (1998).

[35] Zhao G., Wu X., Tan X., Wang X., Sorption of Heavy Metal Ions from Aqueous Solutions: A Review, *The Open Colloid Science Journal*, **4**: 19-31 (2010).

[36] Saeidi M., Ghaemi A., Tahvildari K., Derakhshi P., Exploiting Response Surface Methodology (RSM) as a Novel Approach for the Optimization of Carbon Dioxide Adsorption by Dry Sodium Hydroxide, *Journal of The Chinese Chemical Society*, **65(12)**: 1465-1475 (2018).

[37] Tan Y., Islam M.A., Asif M., Hameed B., Adsorption of Carbon Dioxide by Sodium Hydroxide-Modified Granular Coconut Shell Activated Carbon in a Fixed Bed, *Energy*, **77**: 926-931 (2014).

[38] Gladyshev N., Dvoretskii S., Zhdanov D., Ul'yanova M., Ferapontov Y.A., Choice of a Stabilizer for the Reaction of KOH With Hydrogen Peroxide to Produce Potassium Superoxide, *Russian Journal of Applied Chemistry*, **76(11)**: 1858-1859 (2003).

[39] White M.G., Paris D.T., "Control of Breathing Atmospheres Using Alkali Metal Superoxides: An Engineering Analysis", Georgia Institute of Technology (1981).

[40] Vol′nov I. i. a. I., "Peroxides, Superoxides, and Ozonides of Alkali and Alkaline Earth Metals". Springer, (1966).

[41] Petrocelli A., Kraus D., The Inorganic Superoxides, *Journal of Chemical Education*, **40(3)**: 146 (1963).

[42] Gladysheva T., Gladyshev N., Dvoretskii S., Phase Composition of the Carbonatization Product of Nanocrystalline KO_2 Deposited on a Glass Fiber Matrix, *Inorganic Materials*, **52(5)**: 459-463 (2016).

[43] Cullity B., Stock S., "Elements of X-Ray Diffraction" Prentice-Hall Inc, New York, (2001).

[44] Gladyshev N., Gladysheva T.V., Putin S.B., Dorokhov R.V., Simanenkov E.L., Plotnikov M.Yu., Rodaev V.V., Development of a Nanocrystalline Material for Air Regeneration Devices, *Russian Journal of General Chemistry*, **84(11)**: 2353-2358 (2014).

[45] Brunauer S., Emmett P.H., Teller E., Adsorption of Gases in Multimolecular Layers, *Journal of the American Chemical Society*, **60(2)**: 309-319 (1938).

[46] Dollimore D., Spooner P., Turner A., The BET Method of Analysis of Gas Adsorption Data and Its Relevance to the Calculation of Surface Areas, *Surface Technology*, **4(2)**: 121-160 (1976).

[47] Sing K.S., Reporting Physisorption Data for Gas/Solid Systems with Special Reference to the Determination of Surface Area and Porosity (Recommendations 1984), *Pure and Applied Chemistry*, **57(4)**: 603-619 (1985).

[48] Lowell S., Shields J.E., Thomas M.A., Thommes M., "Characterization of Porous Solids and Powders: Surface Area, Pore Size and Density". Springer Science & Business Media, (2012).

[49] Liu J., Wu L., Chen X., Kinetic Model Investigation on Lead (II) Adsorption Using Silica-Based Hybrid Membranes, *Desalination and Water Treatment*, **54(8)**: 2307-2313 (2015).

[50] Lagergren S., "Zur Theorie Der Sogenannten Adsorption Geloster Stoffe," (1898).

[51] Ammendola P., Raganati F., Chirone R., CO2 Adsorption on a Fine Activated Carbon in a Sound Assisted Fluidized Bed: Thermodynamics and Kinetics, *Chemical Engineering Journal*, **322**: 302-313 (2017).
[52] Bulut E., Ozacar M., Sengil A., Adsorption of Malachite Green onto Bentonite: Equilibrium and Kinethics Studies and Process Design, *Microporous And Mesoporous Materials*, **15**: 234-246 (2008).
[53] Özacar M., Şengil İ. A., A Kinetic Study of Metal Complex Dye Sorption onto Pine Sawdust, *Process Biochemistry*, **40(2)**: 565-572 (2005).
[54] Atia A. A., Donia A. M., Yousif A. M., Removal of Some Hazardous Heavy Metals from Aqueous Solution Using Magnetic Chelating Resin with Iminodiacetate Functionality, *Separation and Purification Technology*, **61(3)**: 348-357 (2008).
[55] Guibal E., Milot C., Tobin J.M., Metal-Anion Sorption by Chitosan Beads: Equilibrium and Kinetic Studies, *Industrial & Engineering Chemistry Research*, **37(4)**: 1454-1463 (1998).
[56] Subha R., Namasivayam C., Modeling of Adsorption Isotherms and Kinetics of 2, 4, 6-Trichlorophenol onto Microporous ZnCl2 Activated Coir Pith Carbon, *J. Environ. Eng. Manage*, **18(4)**: 275-280 (2008).
[57] Ritchie A., Alternative to the Elovich Equation for the Kinetics of Adsorption of Gases on Solids, *Journal of the Chemical Society, Faraday Transactions 1: Physical Chemistry in Condensed Phases*, **73**: 1650-1653 (1977).
[58] Zeldowitsch J., Über den Mechanismus Der Katalytischen Oxydation Von CO an MnO_2, *Acta physicochim. URSS*, **1**: 364-449 (1934).
[59] Weber W. J., Morris J. C., Kinetics of Adsorption on Carbon from Solution, *Journal of the Sanitary Engineering Division*, **89(2)**: 31-60 (1963).
[60] Adelodun A.A., Ngila J.C., Kim D.-G., Jo Y.-M., Isotherm, Thermodynamic and Kinetic Studies of Selective CO2 Adsorption on Chemically Modified Carbon Surfaces, *Aerosol and Air Quality Research*, **16(12)**: 3312-3329 (2016).
[61] Ghaemi A., Torab-Mostaedi M., Ghannadi-Maragheh M., Characterizations of strontium (II) and Barium (II) Adsorption from Aqueous Solutions Using Dolomite Powder, *Journal of Hazardous Materials*, **190(1-3)**: 916-921 (2011).
[62] Bayhan B., Ali K., Length-Weight and Length-Length Relationships of the Salema Sarpa Salpa (Linnaeus, 1758) in Izmir Bay (Aegean Sea of Turkey), *Pakistan Journal of Zoology*, **47(4)**: (2015).
[63] Rashidi N. A., Yusup S., Borhan A., Isotherm and Thermodynamic Analysis of Carbon Dioxide on Activated Carbon, *Procedia Engineering*, **148**: 630-637 (2016).